ESAIM: M2AN 50 (2016) 1035–1055
DOI: 10.1051/m2an/2015062

ESAIM: Mathematical Modelling and Numerical Analysis
www.esaim-m2an.org

A POSTERIORI ANALYSIS OF ITERATIVE ALGORITHMS FOR NAVIER–STOKES PROBLEM

Christine Bernardi[1], Jad Dakroub[1,2], Gihane Mansour[2] and Toni Sayah[2]

Abstract. This work deals with *a posteriori* error estimates for the Navier–Stokes equations. We propose a finite element discretization relying on the Galerkin method and we solve the discrete problem using an iterative method. Two sources of error appear, the discretization error and the linearization error. Balancing these two errors is very important to avoid performing an excessive number of iterations. Several numerical tests are provided to evaluate the efficiency of our indicators.

Mathematics Subject Classification. 65N30, 65N15, 65J15, 76D05.

Received September 10, 2014. Revised September 2, 2015.

1. Introduction

The *a posteriori* analysis controls the overall discretization error of a problem by providing error indicators easy to compute. Once these error indicators are constructed, their efficiency can be proven by bounding each indicator by the local error. This analysis was first introduced by Babuška [3], and developed by Verfürth [27]. The present work investigates *a posteriori* error estimates of the finite element discretization of the Navier–Stokes equations in polygonal domains. In fact, many works have been carried out in this field. In [12], El Akkad, El Khalfi and Guessous proposed a numerical solution of the incompressible Navier–Stokes equations based on an algorithm of discretization by mixed finite elements with *a posteriori* error estimation of the computed solutions. Other works for the *a posteriori* estimation of stationary Navier–Stokes have been introduced in [20, 21, 25]. In [6], Bernardi *et al.* considered a variational formulation of the three-dimensional Navier–Stokes equations with mixed boundary conditions and they proved that it admits a solution if the domain satisfies a suitable regularity assumption. In addition, they established *a priori* and *a posteriori* error estimates. As well, in [17], Ervin *et al.* present locally calculable *a posteriori* error estimators for the basic two-level discretization of the Navier–Stokes equations.

The aim of this paper is to prove that, when two types of indicators are constructed, each of them corresponding to a source of error, balancing these two errors leads to important computational savings. We have decided to use this strategy for the simplest discretization as possible: a Galerkin method relying on finite elements of low degree, a basic linearization algorithm. Indeed, we do think that the arguments that we use here can easily

Keywords and phrases. A posteriori error estimation, Navier–Stokes problem, iterative method.

[1] Laboratoire Jacques-Louis Lions - C.N.R.S. et Université Pierre et Marie Curie, 4 place Jussieu, 75252 Paris cedex 05, France.
[2] Unité de recherche EGFEM, Faculté des sciences, Université Saint-Joseph, Lebanon, Beirut, Liban. bernardi@ann.jussieu.fr; jad.dakroub@usj.edu.lb; gihane.mansour@usj.edu.lb; toni.sayah@usj.edu.lb

Article published by EDP Sciences

be extended to higher order discretizations. But the gain of computation time is more obvious in the simplest one. We apply this strategy on the following Navier–Stokes equations.

Let Ω be a connected open domain in $\mathbb{R}^d$, $d = 2, 3$, with a Lipschitz continuous boundary $\partial\Omega$. We consider, for a positive constant viscosity ν, the following system:

$$\begin{aligned} -\nu\Delta\mathbf{u} + (\mathbf{u}.\nabla)\mathbf{u} + \nabla p &= \mathbf{f} \quad && \text{in } \Omega \\ \operatorname{div} \mathbf{u} &= 0 \quad && \text{in } \Omega \\ \mathbf{u} &= \mathbf{0} \quad && \text{on } \partial\Omega, \end{aligned} \tag{1.1}$$

where the unknowns are the velocity $\mathbf{u}$ and the pressure p of the fluid. The right-hand side $\mathbf{f}$ belongs to $H^{-1}(\Omega)^d$, the dual of the Sobolev space $H_0^1(\Omega)^d$.

Using $\mathcal{P}_1$ Lagrange finite elements for the pressure and $\mathcal{P}_1$-bubble Lagrange finite elements for the velocity, the discrete variational problem amounts to a system of nonlinear equations. In order to solve it we propose an iterative algorithm which consists at each iteration to solve a linearized problem. We establish the corresponding *a posteriori* error estimates. Thus, two sources of error appear, due to linearization and discretization. The main goal of this work is to balance these two sources of error. In fact, if the discretization error dominates then the nonlinear solver iterations are reduced. Therefore, our objective is to calculate *a posteriori* error estimates distinguishing linearization and discretization errors in the context of an adaptive procedure. This type of analysis was introduced by Chaillou and Suri [10, 11] for a general class of problems characterized by strongly monotone operators. It had been developed by El Alaoui *et al.* [13] and by Ern and Vohralík [14], for a class of second-order monotone quasi-linear diffusion-type problems approximated by piecewise affine, continuous finite elements.

In this work we present a strategy for the linearization process. This strategy is iterative and can be outlined as follows:

(1) On the given mesh, perform an iterative linearization until a stopping criterion is satisfied.
(2) If the error is less than the desired precision, then stop, else refine the mesh adaptively and go to step (1).

The outline of the paper is as follows. In Section 2, we present the variational formulation of Navier–Stokes problem (1.1). We introduce in Section 3 the discrete variational problem with the *a priori* error estimate. The iterative algorithm is presented in Section 4. The *a posteriori* analysis of the discretization and of the iterative algorithm is performed in Section 5. Section 6 is devoted to the numerical experiments.

2. Preliminaries

We describe in this section the Navier–Stokes problem (1.1) together with its variational formulation. First of all, we recall the main notion and results which we use later on. For the domain Ω, denote by $L^p(\Omega)$ the space of measurable functions v such that $|v|^p$ is integrable. For $v \in L^p(\Omega)$, the norm is defined by

$$\|v\|_{L^p(\Omega)} = \left(\int_\Omega |v(x)|^p \mathrm{d}\mathbf{x} \right)^{1/p}.$$

We consider the following space

$$X = H_0^1(\Omega)^d = \left\{ \mathbf{v} = (v_i) \in L^2(\Omega)^d; \nabla v_i \in L^2(\Omega)^d;\ \mathbf{v}_{|\partial\Omega} = 0 \right\},$$

and its dual space $H^{-1}(\Omega)^d$.

We denote by $L_0^2(\Omega)$ the space of functions in $L^2(\Omega)$ with zero mean-value on Ω.

$$M = L_0^2(\Omega) = \left\{ q \in L^2(\Omega); \quad \int_\Omega q \, \mathrm{d}\mathbf{x} = 0 \right\}.$$

We recall the Sobolev imbeddings (see Adams [1], Chap. 3).

Lemma 2.1. *For all $j \leq 6$ and $d = 2, 3$, there exists a positive constant S_j such that*

$$\forall v \in H_0^1(\Omega), \quad \|v\|_{L^j(\Omega)} \leq S_j |v|_{1,\Omega}. \tag{2.1}$$

We now assume that the data $\mathbf{f}$ belongs to $H^{-1}(\Omega)^d$. Then the system (1.1) is equivalent to the following variational problem:

Find $\mathbf{u} \in X$, $p \in M$ such that

$$\begin{aligned} \forall \mathbf{v} \in X, \quad a(\mathbf{u}, \mathbf{v}) + c(\mathbf{u}; \mathbf{u}, \mathbf{v}) + b(\mathbf{v}, p) &= \langle \mathbf{f}, \mathbf{v} \rangle, \\ \forall q \in M, \qquad b(\mathbf{u}, q) &= 0, \end{aligned} \tag{2.2}$$

where the bilinear forms $a(.,.)$ and $b(.,.)$ and the trilinear form $c(.,.,.)$ are defined by

$$\begin{aligned} a(\mathbf{u}, \mathbf{v}) &= \nu \int_\Omega \nabla \mathbf{u} \nabla \mathbf{v} \, \mathrm{d}\mathbf{x}, \\ b(\mathbf{v}, q) &= -\int_\Omega q \, \mathrm{div} \, \mathbf{v} \, \mathrm{d}\mathbf{x}, \\ c(\mathbf{w}; \mathbf{u}, \mathbf{v}) &= \int_\Omega (\mathbf{w}.\nabla)\mathbf{u}\mathbf{v} \, \mathrm{d}\mathbf{x}. \end{aligned} \tag{2.3}$$

Furthermore, the bilinear form $b(.,.)$ satisfies the following inf-sup condition (see [18], Chap. I, Eq. (5.14) for instance)

$$\inf_{q \in M, q \neq 0} \sup_{\mathbf{v} \in X} \frac{b(\mathbf{v}, q)}{\|\mathbf{v}\|_X \, \|q\|_M} = \beta > 0. \tag{2.4}$$

The existence and the conditional uniqueness of the solution $(\mathbf{u}, p)$ of problem (2.2) is given in [18] (Chap. IV, Sect. 2). Furthermore, the solution of the problem (2.2) verify the bound:

$$|\mathbf{u}|_{1,\Omega} \leq \frac{c}{\nu} ||\mathbf{f}||_{-1,\Omega}. \tag{2.5}$$

In order to calculate the *a posteriori* error estimate, we introduce the Stokes equations which are defined as follows:

$$\begin{aligned} -\nu \Delta \mathbf{u} + \nabla p &= \mathbf{f} \quad \text{in } \Omega \\ \mathrm{div} \, \mathbf{u} &= 0 \quad \text{in } \Omega \\ \mathbf{u} &= \mathbf{0} \quad \text{on } \partial\Omega. \end{aligned} \tag{2.6}$$

Using the previous notation, the Stokes problem amounts to the following variational form:

Find $\mathbf{u} \in X$, $p \in M$ such that

$$\begin{aligned} \forall \mathbf{v} \in X, \quad a(\mathbf{u}, \mathbf{v}) + b(\mathbf{v}, p) &= \langle \mathbf{f}, \mathbf{v} \rangle, \\ \forall q \in M, \quad b(\mathbf{u}, q) &= 0. \end{aligned} \tag{2.7}$$

The existence and the uniqueness of the solution $(\mathbf{u}, p) \in X \times M$ of problem (2.7) is given in [18] (Chap. I, Sect. 5.1).

Remark 2.2. In the sequel, we denote by C a generic constant that can vary from line to line but is always independent of all discretization parameters.

In what follows, for simplicity reasons, we suppose $d = 2$. In fact, this work can easily be extended to $d = 3$ but requires some more technicalities that we prefer to avoid here.

3. Finite element discretization and the *a priori* estimate

This section collects some useful notation concerning the discrete setting and the *a priori* estimate.

Let $(\mathcal{T}_h)_h$ be a regular family of triangulations of the polygonal domain Ω, in the sense that, for each h:

- The union of all elements of $\mathcal{T}_h$ is equal to $\overline{\Omega}$.
- The intersection of two different elements of $\mathcal{T}_h$, if not empty, is a vertex or a whole edge of both triangles.
- The ratio of the diameter h_K of any element K of $\mathcal{T}_h$ to the diameter of its inscribed circle is smaller than a constant independent of h.

As usual, h stands for the maximum of the diameters h_K, $K \in \mathcal{T}_h$.

Let (X_h, M_h) be the couple of discrete spaces corresponding to (X, M) defined as follow:

$$M_h = \left\{ q_h \in M,\ \forall K \in \mathcal{T}_h,\ q_{h|K} \in \mathcal{P}_1(K) \right\} \quad \text{and} \quad X_h = \left\{ \mathbf{v}_h \in X,\ \forall K \in \mathcal{T}_h,\ \mathbf{v}_{h|K} \in (\mathcal{P}_1(K)\text{-bubble})^2 \right\}$$

where $\mathcal{P}_1(K)$ stands for the space of restrictions to K of affine functions. $\mathcal{P}_1(K)$-bubble is the sum of a polynomial of $\mathcal{P}_1(K)$ and a "bubble" function b_K. Denoting the vertices of K by $a_i, 1 \leq i \leq 3$, and its corresponding barycentric coordinates by λ_i, the basic bubble function b_K is the polynomial of degree three

$$b_K(x) = \lambda_1(x)\lambda_2(x)\lambda_3(x).$$

We observe that $b_K(x) = 0$ on ∂K and that $b_K(x) > 0$ on K. The graph of b_K looks like a bubble attached to the boundary of K, hence its name.

We then consider the following finite element discretization of Navier–Stokes problem (2.2), obtained by the Galerkin method:

Find $\mathbf{u}_h \in X_h$, $p_h \in M_h$ such that

$$\forall \mathbf{v}_h \in X_h,\ \ \nu \int_\Omega \nabla \mathbf{u}_h \nabla \mathbf{v}_h \mathrm{d}\mathbf{x} + \int_\Omega (\mathbf{u}_h.\nabla)\mathbf{u}_h \mathbf{v}_h \mathrm{d}\mathbf{x} - \int_\Omega p_h \mathrm{div}\ \mathbf{v}_h\ \mathrm{d}\mathbf{x} = \langle \mathbf{f}, \mathbf{v}_h \rangle,$$
$$\forall q_h \in M_h,\ \ \int_\Omega q_h \mathrm{div}\ \mathbf{u}_h\ \mathrm{d}\mathbf{x} = 0. \tag{3.1}$$

In order to solve the discrete problem (3.1), we introduce the following space

$$V_h = \left\{ \mathbf{v}_h \in X_h; \forall q_h \in M_h,\ -\int_\Omega q_h \mathrm{div}\ \mathbf{v}_h \mathrm{d}\mathbf{x} = 0 \right\}.$$

Problem (3.1) is then equivalent to the problem:

Find $\mathbf{u}_h \in V_h$ such that

$$\forall \mathbf{v}_h \in V_h,\ \ \nu \int_\Omega \nabla \mathbf{u}_h \nabla \mathbf{v}_h \mathrm{d}\mathbf{x} + \int_\Omega (\mathbf{u}_h.\nabla)\mathbf{u}_h \mathbf{v}_h \mathrm{d}\mathbf{x} = \langle \mathbf{f}, \mathbf{v}_h \rangle, \tag{3.2}$$

and admits at least one solution $(\mathbf{u}_h, p_h) \in X_h \times M_h$ ([18], Chap. IV, Thm. 4.1) such that

$$|\mathbf{u}_h|_{1,\Omega} \leq \frac{c}{\nu} \|\mathbf{f}\|_{-1,\Omega}. \tag{3.3}$$

In addition, if $\mathbf{u} \in H^2(\Omega)^2$ and $p \in H^1(\Omega)$, the *a priori* estimate can be proved by following the approach in [7]. Under some further assumptions, it reads ([18], Chap. IV, Thm. 4.1)

$$|\mathbf{u} - \mathbf{u}_h|_{1,\Omega} + \|p - p_h\|_{0,\Omega} \leq Ch.$$

4. Iterative algorithm

There exist in the literature many iterative algorithms to solve the Navier–Stokes discrete problem. For instance, we refer to [8] for a time dependent discrete problem (even for steady state problem), to [2] for a stabilized finite element method, ... In order to solve the Navier–Stokes discrete problem, we propose in this section a very simple iterative algorithm (see for instance [4]). Since we have used low order finite elements for the discretization, we also choose a low order scheme, in order to reduce the cost of the computation. In fact, we linearize the discrete problem and we set an initial guess $\mathbf{u}_h^0$.

Iterative algorithm. Let $\mathbf{u}_h^0$ be an initial guess. We introduce, for $i \geq 0$, the following algorithm:
Find $\mathbf{u}_h^{i+1} \in X_h$, $p_h^{i+1} \in M_h$ such that

$$\forall \mathbf{v}_h \in X_h, \quad \nu \int_\Omega \nabla \mathbf{u}_h^{i+1} \nabla \mathbf{v}_h \, \mathrm{d}\mathbf{x} + \int_\Omega (\mathbf{u}_h^i . \nabla) \mathbf{u}_h^{i+1} \mathbf{v}_h \, \mathrm{d}\mathbf{x} - \int_\Omega p_h^{i+1} \operatorname{div} \mathbf{v}_h \, \mathrm{d}\mathbf{x} = \langle \mathbf{f}, \mathbf{v}_h \rangle,$$
$$\forall q_h \in M_h, \quad \int_\Omega q_h \operatorname{div} \mathbf{u}_h^{i+1} \, \mathrm{d}\mathbf{x} = 0. \tag{4.1}$$

We clearly see that problem (4.1) has the following form:
Find $\mathbf{u}_h^{i+1} \in V_h$ such that

$$\forall \, \mathbf{v}_h \in V_h, \quad \nu \int_\Omega \nabla \mathbf{u}_h^{i+1} \nabla \mathbf{v}_h \, \mathrm{d}\mathbf{x} + \int_\Omega (\mathbf{u}_h^i . \nabla) \mathbf{u}_h^{i+1} \mathbf{v}_h \, \mathrm{d}\mathbf{x} = \langle \mathbf{f}, \mathbf{v}_h \rangle. \tag{4.2}$$

Remark 4.1. The convergence properties of (4.1) and of more sophisticated linearization algorithms have been proved, see [4] among others. For instance, the convergence is faster for the Newton's method, however it only holds for a very accurate choice of the initial value (even solving a Stokes problem as an initial step can lead to a divergence of the algorithm for high values of the Reynolds number, *i.e.* when the solution of the Navier–Stokes is not unique, see [23], Sect. 4.3.1). In fact, the following technics of *a posteriori* error estimates based on two types of indicators (discretization and linearization) can be followed for almost iterative algorithm.

5. *A posteriori* error analysis

We start this section by introducing some additional notation needed for constructing and analyzing the error indicators in the sequel.

For any element $K \in \mathcal{T}_h$ we denote by $\mathcal{E}(K)$ the set of its edges and we set

$$\mathcal{E}_h = \bigcup_{K \in \mathcal{T}_h} \mathcal{E}(K).$$

With any edge $e \in \mathcal{E}_h$ we associate a unit vector $\mathbf{n}$ such that $\mathbf{n}$ is orthogonal to e. We split $\mathcal{E}(K)$ in the form

$$\mathcal{E}(K) = \mathcal{E}_{K,\partial\Omega} \cup \mathcal{E}_{K,\Omega},$$

where $\mathcal{E}_{K,\partial\Omega}$ is the set of edges in $\mathcal{E}(K)$ that lie on $\partial\Omega$ and $\mathcal{E}_{K,\Omega} = \mathcal{E}(K) \setminus \mathcal{E}_{K,\partial\Omega}$. Furthermore, for $K \in \mathcal{T}_h$ and $e \in \mathcal{E}_h$, let h_K and h_e be their diameter and length respectively. An important tool in the construction of bounds for the total error is Clément's interpolation operator $\mathcal{R}_h$ with values in X_h. The operator $\mathcal{R}_h$ satisfies, for all $v \in H_0^1(\Omega)$, the following local approximation properties (see Verfürth [27], Chap. 1):

$$\|v - R_h v\|_{L^2(K)} \leq C h_K |v|_{1,\Delta_K},$$
$$\|v - R_h v\|_{L^2(e)} \leq C h_e^{1/2} |v|_{1,\Delta_e},$$

where Δ_K and Δ_e are the following sets:

$$\Delta_K = \bigcup \left\{ K' \in \mathcal{T}_h; \;\; K' \cap K \neq \emptyset \right\} \quad \text{and} \quad \Delta_e = \bigcup \left\{ K' \in \mathcal{T}_h; \;\; K' \cap e \neq \emptyset \right\}.$$

We now recall the following properties (see Verfürth [27], Chap. 1): let r be a positive integer. For all $v \in P_r(K)$, the following properties hold

$$C \left\| v \right\|_{L^2(K)} \leq \left\| v b_K^{1/2} \right\|_{L^2(K)} \leq \left\| v \right\|_{L^2(K)} \tag{5.1}$$

$$|v|_{1,K} \leq C h_K^{-1} \left\| v \right\|_{L^2(K)}, \tag{5.2}$$

where b_K is the bubble function of the element K.

Finally, we denote by $[v_h]$ the jump of v_h across the common edge e of two adjacent elements $K, K' \in \mathcal{T}_h$. We have now provided all prerequisites to establish bounds for the total error.

We start the *a posteriori* analysis of the iterative algorithm. In order to prove an upper bound of the error, we first introduce an approximation f_h of the data f which is constant on each element K of $\mathcal{T}_h$. Then, we distinguish the discretization and linearization errors. We first write the weak residual equation.

Let $(\mathbf{u}, p)$ and $(\mathbf{u}_h^i, p_h^i)$ the solution of the (2.2) and (4.1), for all $\mathbf{v} \in X$ and $\mathbf{v}_h \in X_h$, we have:

$$\begin{aligned}
&\nu \int_\Omega \nabla \mathbf{u} \nabla \mathbf{v} \, \mathrm{d}\mathbf{x} + \int_\Omega (\mathbf{u}.\nabla)\mathbf{u}\mathbf{v} \, \mathrm{d}\mathbf{x} - \int_\Omega p \, \mathrm{div} \, \mathbf{v} \, \mathrm{d}\mathbf{x} \\
&\quad - \nu \int_\Omega \nabla \mathbf{u}_h^{i+1} \nabla \mathbf{v} \, \mathrm{d}\mathbf{x} - \int_\Omega (\mathbf{u}_h^i.\nabla)\mathbf{u}_h^{i+1}\mathbf{v} \, \mathrm{d}\mathbf{x} + \int_\Omega p_h^{i+1} \, \mathrm{div} \, \mathbf{v} \, \mathrm{d}\mathbf{x} \\
&\quad = \langle \mathbf{f}, \mathbf{v} - \mathbf{v}_h \rangle - \nu \int_\Omega \nabla \mathbf{u}_h^{i+1} \nabla (\mathbf{v} - \mathbf{v}_h) \, \mathrm{d}\mathbf{x} - \int_\Omega (\mathbf{u}_h^i.\nabla)\mathbf{u}_h^{i+1}(\mathbf{v} - \mathbf{v}_h) \, \mathrm{d}\mathbf{x} + \int_\Omega p_h^{i+1} \, \mathrm{div} \, (\mathbf{v} - \mathbf{v}_h) \, \mathrm{d}\mathbf{x}.
\end{aligned} \tag{5.3}$$

Adding and subtracting $\displaystyle\int_\Omega (\mathbf{u}_h^{i+1}.\nabla)\mathbf{u}_h^{i+1}\mathbf{v} \, \mathrm{d}\mathbf{x}$ and using the Green formula, give

$$\begin{aligned}
&\nu \int_\Omega \nabla \mathbf{u} \nabla \mathbf{v} \, \mathrm{d}\mathbf{x} + \int_\Omega (\mathbf{u}.\nabla)\mathbf{u}\mathbf{v} \, \mathrm{d}\mathbf{x} - \int_\Omega p \mathrm{div} \, \mathbf{v} \, \mathrm{d}\mathbf{x} \\
&-\nu \int_\Omega \nabla \mathbf{u}_h^{i+1} \nabla \mathbf{v} \, \mathrm{d}\mathbf{x} - \int_\Omega (\mathbf{u}_h^{i+1}.\nabla)\mathbf{u}_h^{i+1}\mathbf{v} \, \mathrm{d}\mathbf{x} + \int_\Omega p_h^{i+1} \, \mathrm{div} \, \mathbf{v} \, \mathrm{d}\mathbf{x} \\
&\quad = \sum_{K \in \mathcal{T}_h} \int_K (\mathbf{f} - \mathbf{f}_h)(\mathbf{v} - \mathbf{v}_h) \, \mathrm{d}\mathbf{x} + \sum_{K \in \mathcal{T}_h} \left\{ \int_K (\mathbf{f}_h + \nu \Delta \mathbf{u}_h^{i+1} - (\mathbf{u}_h^i.\nabla)\mathbf{u}_h^{i+1} - \nabla p_h^{i+1})(\mathbf{v} - \mathbf{v}_h) \, \mathrm{d}\mathbf{x} \right. \\
&\quad \left. - \frac{1}{2} \sum_{e \in \mathcal{E}_{K,\Omega}} \int_e \left[\nu \frac{\partial \mathbf{u}_h^{i+1}}{\partial n} - p_h^{i+1} \mathbf{n} \right] .(\mathbf{v} - \mathbf{v}_h) \, \mathrm{d}\tau \right\} + \int_\Omega \left(\left(\mathbf{u}_h^i - \mathbf{u}_h^{i+1} \right) .\nabla \right) \mathbf{u}_h^{i+1} \mathbf{v} \, \mathrm{d}\mathbf{x},
\end{aligned} \tag{5.4}$$

where τ denotes the tangential coordinate on ∂K.

On the other hand, for all $q \in L^2(\Omega)$

$$b(\mathbf{u} - \mathbf{u}_h^{i+1}, q) = \int_\Omega q \mathrm{div} \, \mathbf{u}_h^{i+1} \, \mathrm{d}\mathbf{x}. \tag{5.5}$$

We now define the local linearization indicator $\eta_{K,i}^{(L)}$ and the local discretization indicator $\eta_{K,i}^{(D)}$, corresponding to an element $K \in \mathcal{T}_h$, by:

$$\eta_{K,i}^{(L)} = |\mathbf{u}_h^{i+1} - \mathbf{u}_h^i|_{1,K}, \tag{5.6}$$

$$\eta_{K,i}^{(D)} = h_K \left\|\mathbf{f}_h + \nu\Delta\mathbf{u}_h^{i+1} - (\mathbf{u}_h^i.\nabla)\mathbf{u}_h^{i+1} - \nabla p_h^{i+1}\right\|_{L^2(K)} + \frac{1}{2}\sum_{e\in\mathcal{E}_{K,\Omega}} h_e^{1/2}\left\|\left[\nu\frac{\partial\mathbf{u}_h^{i+1}}{\partial n} - p_h^{i+1}\mathbf{n}\right]\right\|_{L^2(e)} + \left\|\operatorname{div}\mathbf{u}_h^{i+1}\right\|_{L^2(K)}. \tag{5.7}$$

In order to calculate the *a posteriori* error estimates, we denote by $\mathcal{S}$ the operator which associates with any $\mathbf{f}$ in $H^{-1}(\Omega)^d$ the part $\mathbf{w} = \mathbf{u}$ of the solution $(\mathbf{u}, p)$ of the Stokes problem (2.6),

$$\begin{aligned}\mathcal{S} : H^{-1}(\Omega)^d &\to X\\ \mathbf{f} &\mapsto \mathcal{S}\mathbf{f} = \mathbf{w}.\end{aligned}$$

We consider now the following mapping

$$\begin{aligned}G : X &\to H^{-1}(\Omega)^d\\ \mathbf{w} &\mapsto G(\mathbf{w}) = (\mathbf{w}.\nabla)\mathbf{w} - \mathbf{f}\end{aligned}$$

and we observe that problem (2.2) can equivalently be written as

$$F(\mathbf{u}) = \mathbf{u} + SG(\mathbf{u}) = 0. \tag{5.8}$$

Lemma 5.1. *Let $(\mathbf{u}, p)$ be the solution of problem (2.2) and denote by DG the differential of G. There exists a real number $L > 0$, such that the following Lipschitz property holds*

$$\forall \mathbf{w} \in X, \quad \left\|\mathcal{S}\big(DG(\mathbf{u}) - DG(\mathbf{w})\big)\right\|_{\mathcal{L}(H^1(\Omega))} \le L|\mathbf{u} - \mathbf{w}|_{1,\Omega},$$

where $\mathcal{L}(H^1(\Omega))$ is the set of linear continuous functions between $H^1(\Omega)$ and itself.

Proof. We have, for all $\mathbf{w},\ \mathbf{z} \in X$

$$\left\|\mathcal{S}\big(DG(\mathbf{u}).\mathbf{z} - DG(\mathbf{w}).\mathbf{z}\big)\right\|_{1,\Omega} \le \frac{C}{\nu}\left\|DG(\mathbf{u}).\mathbf{z} - DG(\mathbf{w}).\mathbf{z}\right\|_{-1,\Omega}. \tag{5.9}$$

We observe that

$$DG(\mathbf{u}).\mathbf{z} - DG(\mathbf{w}).\mathbf{z} = \mathbf{z}.\nabla(\mathbf{u} - \mathbf{w}) + (\mathbf{u} - \mathbf{w}).\nabla\mathbf{z}, \tag{5.10}$$

hence

$$\left\|\big(DG(\mathbf{u}) - DG(\mathbf{w})\big).\mathbf{z}\right\|_{-1,\Omega} \le 2S_4^2|\mathbf{u} - \mathbf{w}|_{1,\Omega}|\mathbf{z}|_{1,\Omega}. \tag{5.11}$$

Thus, combining (5.9) with (5.10) and (5.11) yields the desired property. □

Assumption 5.2. The solution $(\mathbf{u}, p) \in X \times M$ of problem (2.2) is such that the operator $Id + SDG(\mathbf{u})$ is an isomorphism of X.

Remark 5.3. Assumption 5.2 implies that the solution $\mathbf{u}$ is locally unique, which is weaker than the global uniqueness of the solution.

We can now state the first result of this section:

Theorem 5.4. *Let* $(\mathbf{u}_h^{i+1}, p_h^{i+1}) \in X_h \times M_h$ *and* $(\mathbf{u}_h, p_h) \in X_h \times M_h$ *be the solutions of the iterative problem* (4.1) *and the discrete problem* (3.1)*, respectively. Suppose that the solution* $(\mathbf{u}, p)$ *satisfies Assumption* 5.2*. Then, there exists a neighborhood* $\mathcal{O}$ *of* $\mathbf{u}$ *in* X *such that any solution* $(\mathbf{u}_h^{i+1}, p_h^{i+1})$ *of problem* (4.1) *with* $\mathbf{u}_h^{i+1}$ *in* $\mathcal{O}$ *satisfies the following* a posteriori *error estimate*

$$|\mathbf{u} - \mathbf{u}_h^{i+1}|_{1,\Omega} + \left\|p - p_h^{i+1}\right\|_{L^2(\Omega)} \leq C \left(\sum_{K \in \mathcal{T}_h} \left(\left(\eta_{K,i}^{(D)}\right)^2 + h_K^2 \left\|\mathbf{f} - \mathbf{f}_h\right\|_{L^2(K)}^2 \right) \right)^{1/2} + C' \left(\sum_{K \in \mathcal{T}_h} \left(\eta_{K,i}^{(L)}\right)^2 \right)^{1/2}.$$

Proof. Let $(\mathbf{u}_h^{i+1}, p_h^{i+1}) \in X_h \times M_h$ be the solution of the iterative problem (4.1). We proceed in two steps.

(i) Owing to Lemma 5.1 and Assumption 5.2, it follows from [24] that, for any $\mathbf{u}_h^{i+1}$ in a appropriate neighborhood $\mathcal{O}$ of $\mathbf{u}$

$$|\mathbf{u} - \mathbf{u}_h^{i+1}|_{1,\Omega} \leq C \left\|\mathbf{u}_h^{i+1} + \mathcal{S}G(\mathbf{u}_h^{i+1})\right\|_{-1,\Omega}. \tag{5.12}$$

Introducing $F(\mathbf{u})$ in (5.12) (see Eq. (5.8)), and from equations (5.4) and (5.5), we obtain for all $\mathbf{v}_h \in X_h$

$$|\mathbf{u} - \mathbf{u}_h^{i+1}|_{1,\Omega} \leq C \left(\sup_{\substack{\mathbf{v} \in X \\ \mathbf{v} \neq 0}} \frac{\langle \mathbf{f} - \mathbf{f}_h, \mathbf{v} - \mathbf{v}_h \rangle + \langle \mathcal{J}, \mathbf{v} - \mathbf{v}_h \rangle}{|\mathbf{v}|_{1,\Omega}} + \sup_{\substack{\mathbf{v} \in X \\ \mathbf{v} \neq 0}} \frac{\int_\Omega \left((\mathbf{u}_h^i - \mathbf{u}_h^{i+1}).\nabla\right) \mathbf{u}_h^{i+1} \mathbf{v} \, \mathrm{d}\mathbf{x}}{|\mathbf{v}|_{1,\Omega}} + \sup_{\substack{q \in M \\ q \neq 0}} \frac{\int_\Omega q \, \mathrm{div}\, \mathbf{u}_h^{i+1} \, \mathrm{d}\mathbf{x}}{\|q\|_{L^2(\Omega)}} \right), \tag{5.13}$$

(Note that the last term comes from the definition of $\mathcal{S}$) where

$$\langle \mathcal{J}, \mathbf{v} - \mathbf{v}_h \rangle = \sum_{K \in \mathcal{T}_h} \left\{ \int_K (\mathbf{f}_h + \nu \Delta \mathbf{u}_h^{i+1} - (\mathbf{u}_h^i.\nabla)\mathbf{u}_h^{i+1} - \nabla p_h^{i+1})(\mathbf{v} - \mathbf{v}_h) \, \mathrm{d}\mathbf{x} - \frac{1}{2} \sum_{e \in \mathcal{E}_{K,\Omega}} \int_e \left[\nu \frac{\partial \mathbf{u}_h^{i+1}}{\partial n} - p_h^{i+1} \mathbf{n} \right] . (\mathbf{v} - \mathbf{v}_h) \, \mathrm{d}\tau \right\}.$$

Taking $\mathbf{v}_h$ equal to the image $\mathcal{R}_h \mathbf{v}$ of $\mathbf{v}$ by the Clément operator in (5.13), we obtain the desired estimate for $|\mathbf{u} - \mathbf{u}_h^{i+1}|_{1,\Omega}$.

(ii) Computing $b(\mathbf{v}, p - p_h^{i+1})$ from (5.4) and adding and substracting $\int_\Omega (\mathbf{u}_h^{i+1}.\nabla)\mathbf{u}\mathbf{v} \, \mathrm{d}\mathbf{x}$ we obtain

$$\begin{aligned} b(\mathbf{v}, p - p_h^{i+1}) = {} & \nu \int_\Omega \nabla(\mathbf{u}_h^{i+1} - \mathbf{u}) \nabla \mathbf{v} \, \mathrm{d}\mathbf{x} + \int_\Omega (\mathbf{u}_h^{i+1}.\nabla)(\mathbf{u}_h^{i+1} - \mathbf{u}) \mathbf{v} \, \mathrm{d}\mathbf{x} + \int_\Omega (\mathbf{u}_h^{i+1} - \mathbf{u}) \nabla \mathbf{u} \mathbf{v} \, \mathrm{d}\mathbf{x} \\ & + \sum_{K \in \mathcal{T}_h} \int_K (\mathbf{f} - \mathbf{f}_h)(\mathbf{v} - \mathbf{v}_h) \, \mathrm{d}\mathbf{x} + \sum_{K \in \mathcal{T}_h} \left\{ \int_K (\mathbf{f}_h + \nu \Delta \mathbf{u}_h^{i+1} - (\mathbf{u}_h^i.\nabla)\mathbf{u}_h^{i+1} - \nabla p_h^{i+1})(\mathbf{v} - \mathbf{v}_h) \, \mathrm{d}\mathbf{x} \right. \\ & \left. - \frac{1}{2} \sum_{e \in \mathcal{E}_{K,\Omega}} \int_e \left[\nu \frac{\partial \mathbf{u}_h^{i+1}}{\partial n} - p_h^{i+1} \mathbf{n} \right] . (\mathbf{v} - \mathbf{v}_h) \, \mathrm{d}\tau \right\} + \int_\Omega \left((\mathbf{u}_h^i - \mathbf{u}_h^{i+1}).\nabla\right) \mathbf{u}_h^{i+1} \mathbf{v} \, \mathrm{d}\mathbf{x}. \end{aligned} \tag{5.14}$$

Using Cauchy–Schwarz inequality, (2.5) and (3.3), we derive the following estimate

$$b(\mathbf{v}, p-p_h^{i+1}) \leq \sum_{K\in\mathcal{T}_h}\left(\|\mathbf{f}-\mathbf{f}_h\|_{L^2(K)}+\left\|\mathbf{f}_h+\nu\Delta\mathbf{u}_h^{i+1}-(\mathbf{u}_h^i.\nabla)\mathbf{u}_h^{i+1}-\nabla p_h^{i+1}\right\|_{L^2(K)}\right)\|\mathbf{v}-\mathbf{v}_h\|_{L^2(K)}$$
$$+\frac{1}{2}\sum_{e\in\mathcal{E}_{K,\Omega}}\left\|\left[\nu\frac{\partial\mathbf{u}_h^{i+1}}{\partial n}-p_h^{i+1}\mathbf{n}\right]\right\|_{L^2(e)}\|\mathbf{v}-\mathbf{v}_h\|_{L^2(e)}+\frac{CS_4^2}{\nu}\|\mathbf{f}\|_{0,\Omega}\,|\mathbf{u}_h^{i+1}-\mathbf{u}_h^i|_{1,\Omega}|\mathbf{v}|_{1,\Omega}$$
$$+\left(2\frac{CS_4^2}{\nu}\|\mathbf{f}\|_{0,\Omega}+\nu\right)|\mathbf{u}_h^{i+1}-\mathbf{u}|_{1,\Omega}|\mathbf{v}|_{1,\Omega}. \tag{5.15}$$

Taking $\mathbf{v}_h$ equal $\mathcal{R}_h\mathbf{v}$ in (5.15) and using the inf-sup condition (2.4), we obtain the desired estimate for $\|p-p_h^{i+1}\|_{L^2(\Omega)}$. □

We address now the efficiency of the previous indicators.

Theorem 5.5. *For each $K\in\mathcal{T}_h$, the following estimates hold for the indicators $\eta_{K,i}^{(L)}$ defined in (5.6)*

$$\eta_{K,i}^{(L)} \leq \|\mathbf{u}-\mathbf{u}_h^{i+1}\|_{1,K}+\|\mathbf{u}-\mathbf{u}_h^i\|_{1,K}, \tag{5.16}$$

and for the indicators $\eta_{K,i}^{(D)}$ defined in (5.7)

$$\eta_{K,i}^{(D)} \leq C\left(\eta_{K,i}^{(L)}+\|\mathbf{u}-\mathbf{u}_h^{i+1}\|_{1,\omega_K}+\|p_h^{i+1}-p\|_{L^2(\omega_K)}+\sum_{\kappa\subset\omega_K}h_\kappa\|\mathbf{f}-\mathbf{f}_h\|_{L^2(\kappa)}\right), \tag{5.17}$$

where ω_K is the union of the elements sharing at least one edge with K.

Proof. The estimation of the linearization indicator follows easily from the triangle inequality by introducing $\mathbf{u}$ in $\eta_{K,i}^{(L)}$. We now estimate the discretization indicator $\eta_{K,i}^{(D)}$. We proceed in two steps:

(i) We start by taking $\mathbf{v}_h=0$ and by adding and subtracting $\int_\Omega(\mathbf{u}_h^{i+1}.\nabla)\mathbf{u}\mathbf{v}\,d\mathbf{x}$ in (5.3). We obtain

$$\sum_{K\in\mathcal{T}_h}\left(\int_K(\mathbf{f}_h+\nu\Delta\mathbf{u}_h^{i+1}-(\mathbf{u}_h^i.\nabla)\mathbf{u}_h^{i+1}-\nabla p_h^{i+1})\mathbf{v}\right)d\mathbf{x}=\nu\int_\Omega\nabla(\mathbf{u}-\mathbf{u}_h^{i+1})\nabla\mathbf{v}\,d\mathbf{x}$$
$$+\int_\Omega\big((\mathbf{u}-\mathbf{u}_h^{i+1}).\nabla\big)\mathbf{u}\mathbf{v}\,d\mathbf{x}-\sum_{K\in\mathcal{T}_h}\int_K(\mathbf{f}-\mathbf{f}_h)\mathbf{v}\,d\mathbf{x}+\frac{1}{2}\sum_{e\in\mathcal{E}_{K,\Omega}}\int_e\left[\nu\frac{\partial\mathbf{u}_h^{i+1}}{\partial n}-p_h^{i+1}\mathbf{n}\right].\mathbf{v}\,d\tau\Bigg\}$$
$$+\int_\Omega\big(\mathbf{u}_h^{i+1}.\nabla\big)(\mathbf{u}-\mathbf{u}_h^{i+1})\mathbf{v}\,d\mathbf{x}+\int_\Omega\big((\mathbf{u}_h^{i+1}-\mathbf{u}_h^i).\nabla\big)\mathbf{u}_h^{i+1}\mathbf{v}\,d\mathbf{x}+\int_\Omega(p_h^{i+1}-p)\,\mathrm{div}\,\mathbf{v}\,d\mathbf{x}. \tag{5.18}$$

We choose $\mathbf{v}=\mathbf{v}_K$ such that

$$\mathbf{v}_K=\begin{cases}(\mathbf{f}_h+\nu\Delta\mathbf{u}_h^{i+1}-(\mathbf{u}_h^i.\nabla)\mathbf{u}_h^{i+1}-\nabla p_h^{i+1})b_K & \text{on } K\\ 0 & \text{on } \Omega\setminus K,\end{cases}$$

where b_K is the bubble function of the element K.
Using Cauchy–Schwarz inequality, (5.1) and (5.2) we obtain

$$h_K\left\|\mathbf{f}_h+\nu\Delta\mathbf{u}_h^{i+1}-(\mathbf{u}_h^i.\nabla)\mathbf{u}_h^{i+1}-\nabla p_h^{i+1}\right\|_{L^2(K)}^2$$
$$\leq C\Big(\|\mathbf{u}-\mathbf{u}_h^{i+1}\|_{1,K}\|\mathbf{v}_K\|_{L^2(K)}+h_K\|\mathbf{f}-\mathbf{f}_h\|_{L^2(K)}\|\mathbf{v}_K\|_{L^2(K)}$$
$$+\|p_h^{i+1}-p\|_{L^2(K)}\|\mathbf{v}_K\|_{L^2(K)}+\|\mathbf{u}_h^i-\mathbf{u}_h^{i+1}\|_{1,K}\|\mathbf{v}_K\|_{L^2(K)}\Big). \tag{5.19}$$

Therefore, we obtain the following estimate of the first term of the local discretization estimator $\eta_{K,i}^{(D)}$

$$h_K \left\|\mathbf{f}_h + \nu\Delta\mathbf{u}_h^{i+1} - (\mathbf{u}_h^i.\nabla)\mathbf{u}_h^{i+1} - \nabla p_h^{i+1}\right\|_{L^2(K)} \leq C\left(\left\|\mathbf{u} - \mathbf{u}_h^{i+1}\right\|_{1,K} + h_K \left\|\mathbf{f} - \mathbf{f}_h\right\|_{L^2(K)} + \left\|p_h^{i+1} - p\right\|_{L^2(K)} + \eta_{K,i}^{(L)}\right). \quad (5.20)$$

(ii) We now estimate the second term of $\eta_{K,i}^{(D)}$. Rewriting (5.18), we infer

$$\begin{aligned}\frac{1}{2}\sum_{e\in\mathcal{E}_{K,\Omega}}\int_e\left[\nu\frac{\partial\mathbf{u}_h^{i+1}}{\partial n} - p_h^{i+1}\mathbf{n}\right].\mathbf{v}\,\mathrm{d}\tau &= \sum_{K\in\mathcal{T}_h}\int_K(\mathbf{f}_h + \nu\Delta\mathbf{u}_h^{i+1} - (\mathbf{u}_h^i.\nabla)\mathbf{u}_h^{i+1} - \nabla p_h^{i+1})\mathbf{v}\,\mathrm{d}\mathbf{x}\\ &+ \nu\int_\Omega\nabla(\mathbf{u}_h^{i+1} - \mathbf{u})\nabla\mathbf{v}\,\mathrm{d}\mathbf{x} + \int_\Omega\left((\mathbf{u}_h^{i+1} - \mathbf{u}).\nabla\right)\mathbf{u}\mathbf{v}\,\mathrm{d}\mathbf{x} + \sum_{K\in\mathcal{T}_h}\int_K(\mathbf{f} - \mathbf{f}_h)\mathbf{v}\,\mathrm{d}\mathbf{x}\\ &+ \int_\Omega(\mathbf{u}_h^{i+1}.\nabla)(\mathbf{u}_h^{i+1} - \mathbf{u})\mathbf{v}\,\mathrm{d}\mathbf{x} + \int_\Omega\left((\mathbf{u}_h^i - \mathbf{u}_h^{i+1}).\nabla\right)\mathbf{u}_h^{i+1}\mathbf{v}\mathrm{d}\mathbf{x}\\ &+ \int_\Omega(p - p_h^{i+1})\,\mathrm{div}\,\mathbf{v}\,\mathrm{d}\mathbf{x}. \end{aligned} \quad (5.21)$$

We choose $\mathbf{v} = \mathbf{v}_e$ such that

$$\mathbf{v}_e = \begin{cases} L_{e,\kappa}\left(\left[\dfrac{\partial\mathbf{u}_h^{i+1}}{\partial n} - p_h^{i+1}\mathbf{n}\right]b_e\right) & \kappa\in\{K,K'\}\\ 0 & \text{on } \Omega\setminus(K\cup K')\end{cases}$$

where b_e is the edge-bubble function, K' denotes the other element of $\mathcal{T}_h$ that share e with K and $L_{e,\kappa}$ is a lifting operator from e into κ mapping polynomials vanishing on ∂e into polynomials vanishing in $\partial\kappa\backslash e$ and constructed from a fixed operator on the reference element (see Verfürth [27]). Furthermore, we have for all $v\in P_r(e)$, the following properties

$$C\left\|v\right\|_{L^2(e)} \leq \left\|vb_e^{1/2}\right\|_{L^2(e)} \leq \left\|v\right\|_{L^2(e)}, \quad (5.22)$$

and

$$||L_{e,\kappa}v||_{L^2(\kappa)} + h_e|L_{e,\kappa}v|_{1,\kappa} \leq Ch_e^{1/2}\left\|v\right\|_{L^2(e)}. \quad (5.23)$$

Using Cauchy–Schwarz inequality, (5.22) and (5.23) we get

$$\begin{aligned}h_e^{1/2}\left\|\left[\frac{\partial\mathbf{u}_h^{i+1}}{\partial n} - p_h^{i+1}\mathbf{n}\right]\right\|_{L^2(e)}^2 &\leq (\nu + \frac{2C}{\nu}\left\|\mathbf{f}\right\|_{0,\Omega})\left\|\mathbf{u} - \mathbf{u}_h^{i+1}\right\|_{1,K\cup K'}\left\|\mathbf{v}_e\right\|_{L^2(e)} + h_e\left\|\mathbf{f} - \mathbf{f}_h\right\|_{L^2(K\cup K')}\left\|\mathbf{v}_e\right\|_{L^2(e)}\\ &+ h_e\left\|\mathbf{f}_h + \nu\Delta\mathbf{u}_h^{i+1} - (\mathbf{u}_h^i.\nabla)\mathbf{u}_h^{i+1} - \nabla p_h^{i+1}\right\|_{L^2(K\cup K')}\left\|\mathbf{v}_e\right\|_{L^2(e)}\\ &+ \left\|p_h^{i+1} - p\right\|_{L^2(K\cup K')}\left\|\mathbf{v}_e\right\|_{L^2(e)} + \frac{C}{\nu}\left\|\mathbf{f}\right\|_{0,\Omega}\eta_{K,i}^{(L)}\left\|\mathbf{v}_e\right\|_{L^2(e)}, \end{aligned} \quad (5.24)$$

with

$$\left\|\mathbf{v}_e\right\|_{L^2(e)} \leq c\left\|\left[\nu\frac{\partial\mathbf{u}_h^{i+1}}{\partial n} - p_h^{i+1}\mathbf{n}\right]\right\|_{L^2(e)}.$$

Thus, we have estimated the second term of the local discretization indicator $\eta_{K,i}^{(D)}$.

(iii) Finally, we take $q = q_K$ in (5.5) such that

$$q_K = \begin{cases} \operatorname{div} \mathbf{u}_h^{i+1} & \text{on } K \\ 0 & \text{on } \Omega \setminus K \end{cases}$$

We obtain

$$\left\|\operatorname{div} \mathbf{u}_h^{i+1}\right\|_{L^2(K)} \leq \left\|\mathbf{u} - \mathbf{u}_h^{i+1}\right\|_{1,K}. \tag{5.25}$$

Collecting the bounds above leads to the final result

$$\eta_{K,i}^{(D)} \leq C \left(\left\|\mathbf{u} - \mathbf{u}_h^{i+1}\right\|_{1,\omega_K} + \left\|p - p_h^{i+1}\right\|_{L^2(\kappa)} + \sum_{\kappa \subset \omega_K} h_\kappa \left\|\mathbf{f} - \mathbf{f}_h\right\|_{L^2(\kappa)} + \eta_{K,i}^{(L)} \right). \qquad \square$$

Corollary 5.6. *If we use the following local stopping criteria (proceeding as in* [13] *or* [14]*)*

$$\eta_{K,i}^{(L)} \leq \gamma_K \eta_{K,i}^{(D)}, \quad \forall K \in \mathcal{T}_h,$$

where γ_K is a positive parameter corresponding to the element K such that $\gamma_K C < 1$ (C is the constant of the previous theorem), we have

$$\eta_{K,i}^{(D)} \leq c \left(\left\|\mathbf{u} - \mathbf{u}_h^{i+1}\right\|_{1,\omega_K} + \left\|p_h^{i+1} - p\right\|_{L^2(\omega_K)} + \sum_{\kappa \subset \omega_K} h_\kappa \left\|\mathbf{f} - \mathbf{f}_h\right\|_{L^2(\kappa)} \right).$$

According to standard criteria, these estimates of the local linearization and discretization indicators are fully optimal [27]. In fact we observe that, up to the terms involving the data, the error is bounded by a constant times the sum of all indicators. As well, the indicators are bounded by the error in a neighborhood of K or e.

Instead the local stopping criteria introduced in the previous corollary, we can introduce a global one. In fact we introduce the global linearization error indicator $\eta_i^{(L)}$ and discretization error indicator $\eta_i^{(D)}$ defined by

$$\eta_i^{(L)} = \left(\sum_{K \in \mathcal{T}_h} \left(\eta_{K,i}^{(L)}\right)^2 \right)^{1/2},$$

$$\eta_i^{(D)} = \left(\sum_{K \in \mathcal{T}_h} \left(\eta_{K,i}^{(D)}\right)^2 \right)^{1/2}.$$

Corollary 5.7. *If we use the following global stopping criterion (proceeding as in* [13] *or* [14]*)*

$$\eta_i^{(L)} \leq \gamma \eta_i^{(D)},$$

where γ is a positive parameter such that $\gamma C < 1$ (C is the constant of the previous theorem), we have

$$\eta_i^{(D)} \leq c \left(\left\|\mathbf{u} - \mathbf{u}_h^{i+1}\right\|_{1,\Omega} + \left\|p_h^{i+1} - p\right\|_{L^2(\Omega)} + \sum_{K \subset \Omega} h_K \left\|\mathbf{f} - \mathbf{f}_h\right\|_{L^2(K)} \right).$$

6. Numerical results

In this section, we present numerical results for the Navier–Stokes iterative algorithm. These simulations have been performed using the code FreeFem++ due to Hecht and Pironneau, see [19]. In all this section, $\mathbf{u}_h^0$ is the solution of the Stokes problem with corresponding boundary conditions.

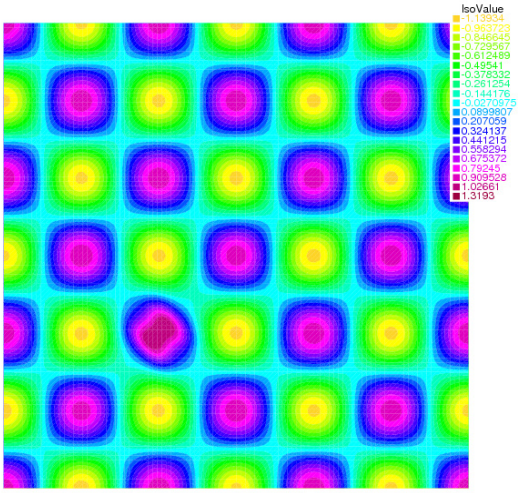

FIGURE 1. Numerical pressure.

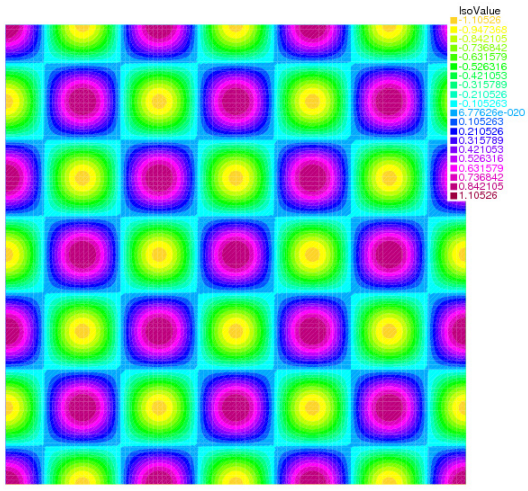

FIGURE 2. Exact pressure.

6.1. *A priori* estimation

We consider the square $\Omega =]0,3[^2$. Each edge is divided into N equal segments so that Ω is divided into $2N^2$ triangles. We consider the iterative Navier–Stokes algorithm and the theoretical solution $(\mathbf{u}, p) = (\text{rot}\,\psi, p)$ where ψ and p are defined as follows

$$\psi(x,y) = \mathrm{e}^{-30\left((x-1)^2+(y-1)^2\right)},$$
$$p(x,y) = \cos(2\pi x)\cos(2\pi y).$$

The convergence criterion used in this section is the following

$$\frac{|\mathbf{u}-\mathbf{u}_h^i|_{1,\Omega}}{|\mathbf{u}|_{1,\Omega}} \leq 10^{-8}.$$

Figures 1 and 2 compare the exact and the numerical solution of the pressure p for $N = 100$. We can see that the two solutions are visually similar.

As well, Figures 3–6 compare the different components of the numerical and exact solutions of the velocity $\mathbf{u}$ for $N = 100$.

Figures 7 and 8 present the error curves (after convergence of the iterative solution) of the velocity ($|\mathbf{u}-\mathbf{u}_h|_{1,\Omega}$) and the pressure ($||p-p_h||_{L^2(\Omega)}$) as a function of $h = \dfrac{1}{N}$ in logarithmic scales. We test the algorithm for the number of segments N going from 60 to 100. The slope of the velocity error curve is equal to 0.92 while it is 1.08 for the pressure error curve.

Remark 6.1. Note that the error curves of the pressure and the velocity are coherent with the theoretical results in Section 3.

6.2. *A posteriori* analysis

In this section, we test our *a posteriori* error estimates on the iterative Navier–Stokes problem. We will present two examples: the first one considers the homogeneous boundary condition and the second one treats the Lid-Driven Cavity.

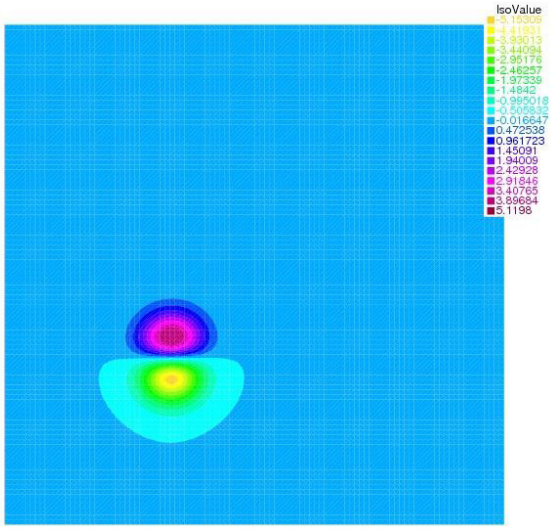

FIGURE 3. First component of the numerical velocity.

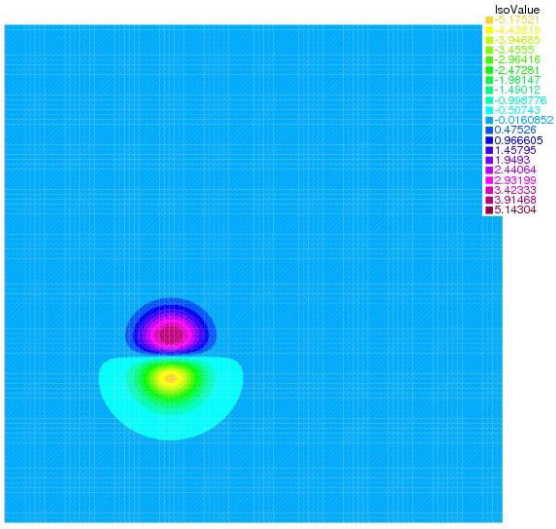

FIGURE 4. First component of the exact velocity.

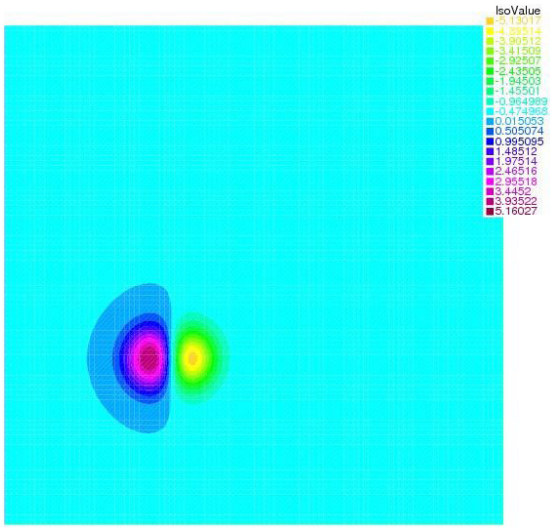

FIGURE 5. Second component of the numerical velocity.

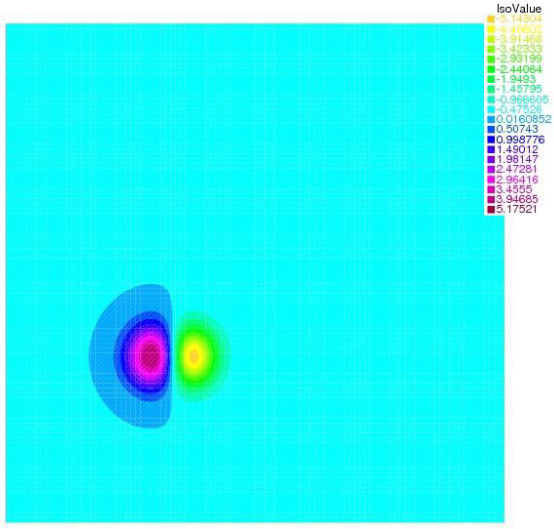

FIGURE 6. Second component of the exact velocity.

6.2.1. First test case

We consider the same domain as previously and the exact solution $(\mathbf{u}, p) = (\text{rot } \psi, p)$ where ψ and p are defined as follows

$$\psi(x,y) = \mathrm{e}^{-30\left((x-1)^2+(y-1)^2\right)},$$
$$p(x,y) = \cos\left(\frac{2\pi}{3}x\right)\cos\left(\frac{2\pi}{3}y\right).$$

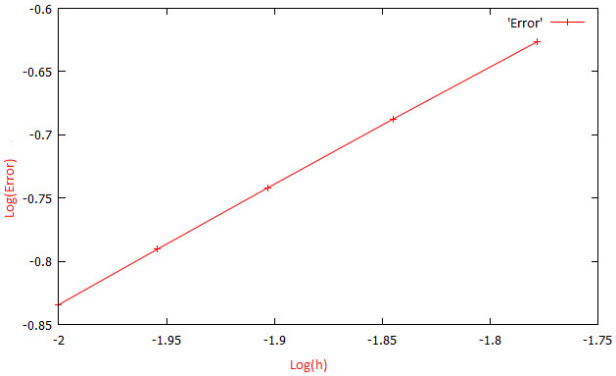

FIGURE 7. Error curve of the velocity ($|\mathbf{u}-\mathbf{u}_h|_{1,\Omega}$) *versus* the size of the mesh $h = \dfrac{1}{N}$, for N going from 60 to 100.

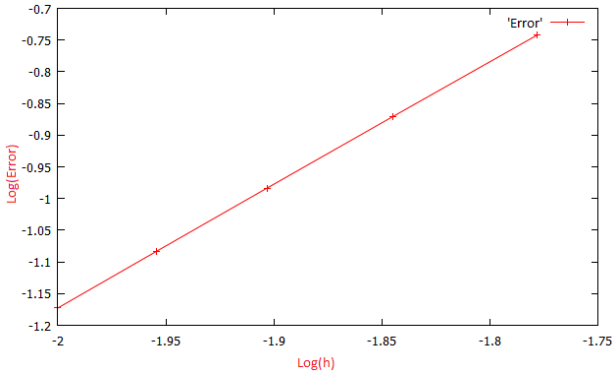

FIGURE 8. Error curve of the pressure ($||p-p_h||_{L^2(\Omega)}$) *versus* the size of the mesh $h = \dfrac{1}{N}$, for N going from 60 to 100.

The considered exact pressure is slightly different than that in the previous section which was constituted of three period in every dimension. In order to show the efficiency of the adapted mesh method according to the velocity, we consider the pressure with one period in every dimension.

We define two different global stopping criteria:

$$\eta_i^{(L)} \leq 10^{-5} \quad \text{Classical stopping criterion,} \tag{6.1}$$

and

$$\eta_i^{(L)} \leq \gamma \eta_i^{(D)} \quad \text{New stopping criterion,} \tag{6.2}$$

where γ is a positive parameter which balances the discretization and linearization errors. In [13,14], the authors introduce this new stopping criterion and choose in practice $\gamma = 0.1$ in their numerical experiments. In this work, we choose $\gamma = 0.01$ for our numerical applications.

Remark 6.2. In [13,14], the authors show numerical experiments corresponding to the local stopping criterion (Cor. 5.6) and the global one (Cor. 5.7). To compare with the classical stopping criterion (6.1), the global one (6.2) is more suitable than local one (Cor. 5.6). Furthermore, it is shown in [13] that (6.2) can be a good criterion for the adaptive method.

Figures 9 to 12 show the evolution of the mesh (see [27], Introduction) using the iterative Navier–Stokes algorithm. We remark that, from an iteration to an other, the mesh is mainly refined in the region where the velocity takes its higher values. An adaptive mesh refinement can be outlined as follows:

(1) Given u_h^i,
  (a) Solve the problem (4.1) to compute u_h^{i+1}.
  (b) Calculate $\eta_i^{(D)}$ and $\eta_i^{(L)}$.
(2) If the stopping criterion (6.2) is satisfied, go to (3), else set $u_h^i = u_h^{i+1}$ and go to (1).
(3)
  (a) If $\eta_i^{(D)}$ is smaller than a fixed error tolerance ε, we stop the iterations and the algorithm.
  (b) Else we adapt the mesh using the indicators $\eta_{K,i}^{(D)}$.
(4) Set $i = i+1$ and go to (1).

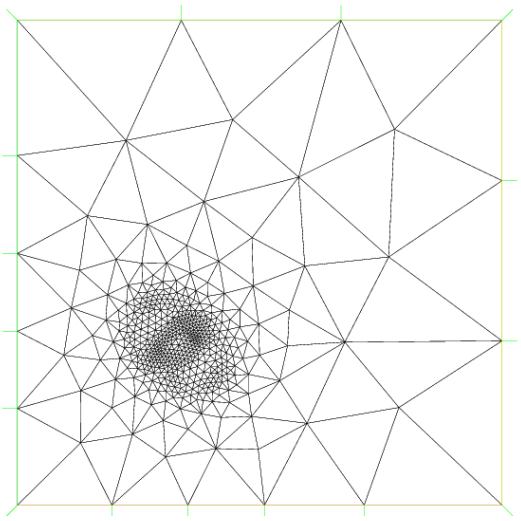

FIGURE 9. 273 vertices.

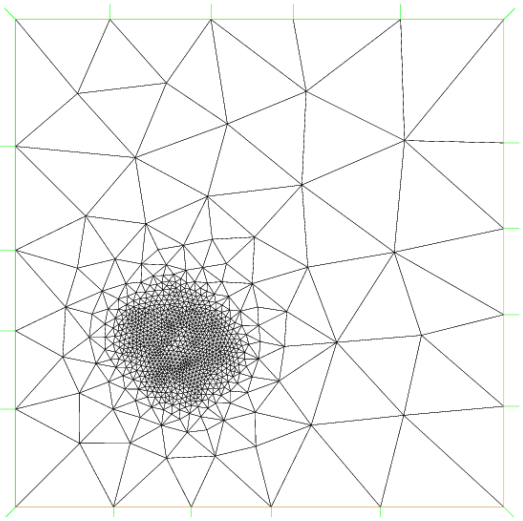

FIGURE 10. 507 vertices.

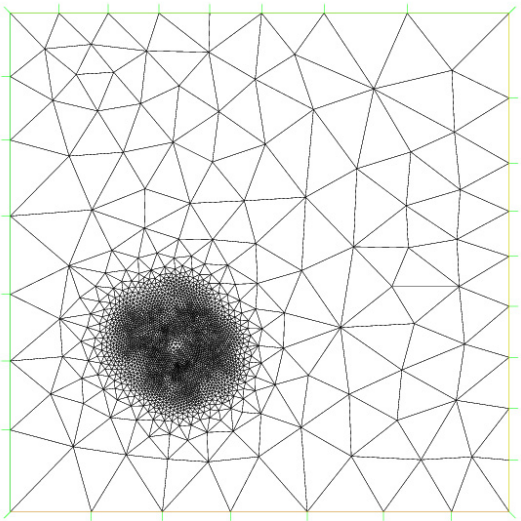

FIGURE 11. 891 vertices.

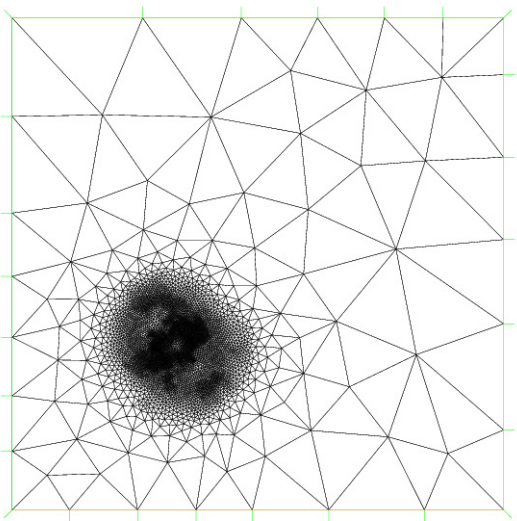

FIGURE 12. 1615 vertices.

In the previous algorithm, the adapt mesh technics is performed by using the "FreeFem++" software (see [19]) and based on the calculated indicators $\eta_{K,i}^{(D)}$. The main idea can be summarized as follow: we calculate the mean value η_i^* of the indicators $\eta_{K,i}^{(D)}$ at each step i, detect the elements of the mesh where the corresponding indicators are larger then η_i^* and refine them.

Figures 13 and 14 present the numerical and the exact first component of the velocity for the mesh refinement of Figure 12.

We observe that the numerical velocity and the exact velocity are visually similar.

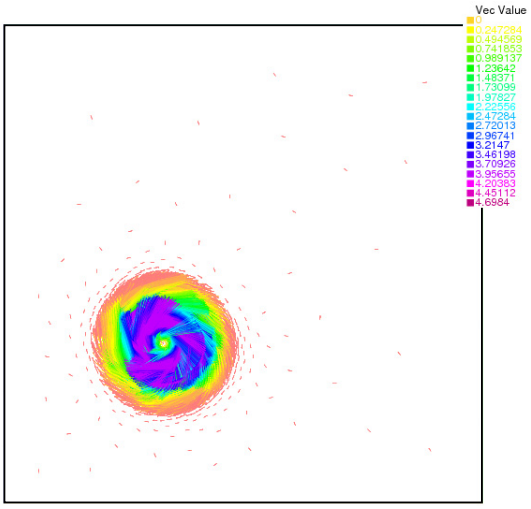

FIGURE 13. Numerical velocity.

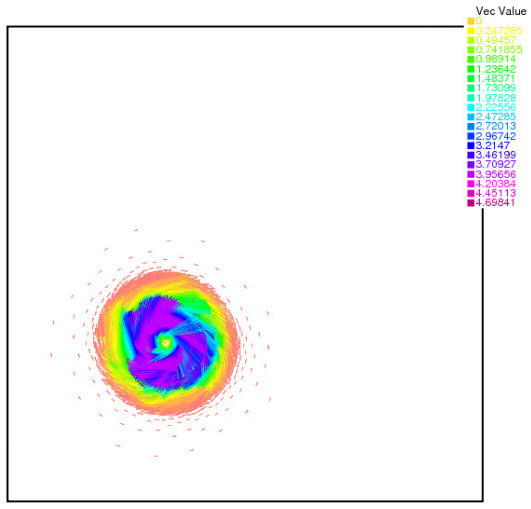

FIGURE 14. Exact velocity.

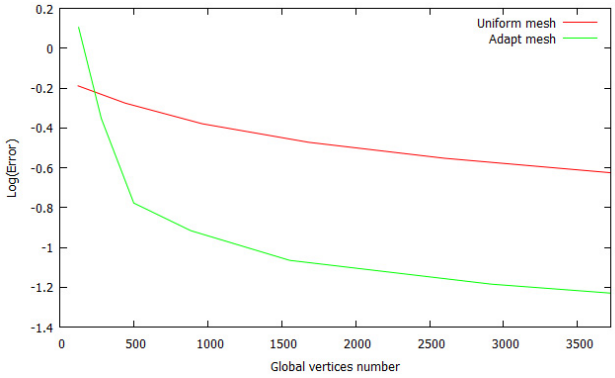

FIGURE 15. Curve of the error E_r as a function of the global vertices number. Uniform mesh (*top*), adaptive mesh (*bottom*).

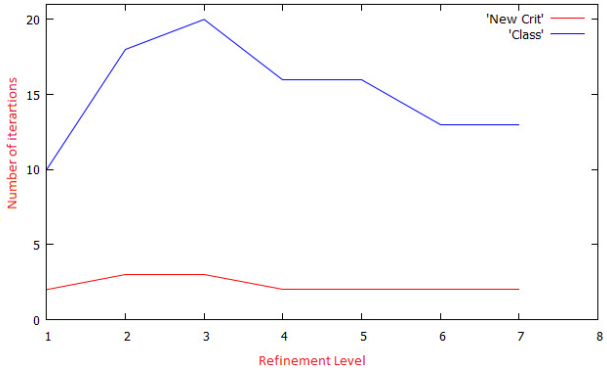

FIGURE 16. Iterations number as a function of the refinement level. Classical criterion (*top*), new criterion (*bottom*).

Figure 15 presents the curve of the error $E_r = \dfrac{|\mathbf{u}-\mathbf{u}_h|_{1,\Omega}}{|\mathbf{u}|_{1,\Omega}}$ (after convergence of the iterative solution) for uniform (red) and adaptive (blue) mesh refinement using the new stopping criterion. We note that the error using an adaptive mesh is much smaller than the error using a uniform mesh.

Figure 16 illustrates the performance of our new stopping criterion with $\gamma = 0.01$ by comparing it to the classical stopping criterion $\eta_i^{(L)} \leq 10^{-5}$. We can clearly observe that our new stopping criterion reduces the number of iterations.

In Tables 1 and 2, we present the effectivity index defined as

$$EI = \left(\frac{\left(\eta_i^{(L)}\right)^2 + \left(\eta_i^{(D)}\right)^2}{|\mathbf{u}_h^i - \mathbf{u}|_{1,\Omega}^2} \right)^{1/2} \simeq \frac{\eta_i^{(D)}}{|\mathbf{u}_h^i - \mathbf{u}|_{1,\Omega}}$$

TABLE 1. Repartition of errors and EI with respect to the iterations for the new stoping criterion.

NK	$i=1$ 150 vertices	$i=2$ 338 vertices	$i=3$ 830 vertices	$i=4$ 2302 vertices	$i=5$ 5109 vertices	$i=6$ 9869
$\frac{\lvert u-u_h^i\rvert_{1,\Omega}}{\lvert u\rvert_{1,\Omega}}$	0.202505	0.141114	0.106995	0.0770237	0.0533372	0.0380128
EI (with (6.2))	5.196	4.6017	4.3130	4.158	4.1656	4.1606

TABLE 2. Repartition of errors and EI with respect to the iterations for the classical stoping criterion.

NK	$i=1$ 149 vertices	$i=2$ 331 vertices	$i=3$ 830 vertices	$i=4$ 2288 vertices	$i=5$ 5180 vertices	$i=6$ 9795
$\frac{\lvert u-u_h^i\rvert_{1,\Omega}}{\lvert u\rvert_{1,\Omega}}$	0.203689	0.137318	0.107731	0.07809	0.0547675	0.0380982
EI (with (6.1))	5.2357	4.6930	4.3082	4.1733	4.1745	4.1793

TABLE 3. CPU time for both criteria.

Method \ Level of refinement	3	4	5	6	7
New criterion	6.466s	8.331s	14.439s	11.591s	15.351s
Classical criterion	30.609s	13.104s	21.279s	29.25s	49.483s

with respect to the number of unknowns NK during the iterations and for the new and classical stopping criteria. We remark that both of these criteria gives the same precision.

Finally, Table 3 presents the CPU time of each level of refinement for both criteria, the classical one and the new one. We can see clearly the efficiency of the new stopping criterion with $\gamma = 0.01$.

6.2.2. Second test case: Lid Driven cavity

In this section, we consider $\Omega =]0,1[^2$, recall that $\nu = \dfrac{1}{Re}$ where Re is the Reynold number and complete the Navier–Stokes equations with the following boundary conditions: $\mathbf{u} = (1,0)$ on the lid (top of Ω) and $\mathbf{u} = (0,0)$ on the sides and the bottom of Ω.

The Lid Driven Cavity is treated in several works. Kawaguti [22] appears to have the earliest numerical solutions for the lid-driven cavity problem by using the stream function-vorticity formulation with a finite difference method. Then, we can cite the works of [9,16,26] which improved the work of Kawaguti. In addition, Barrgy and Carey [5] use the stream function-vorticity formulation but with finite element method. Finally, we can also refer to [8,15]. In this work, we will elaborate numerical results using the adaptive mesh method and give some numerical comparisons of the stream function ψ such that $\mathbf{u} = \mathbf{curl}\,\psi$ which verifies the following variational problem

$$\begin{cases} \text{Find } \psi \in H_0^1(\Omega) \text{ such that for all } \phi \in H_0^1(\Omega) \text{ we have} \\ \displaystyle\int_\Omega \nabla\psi\,\nabla\phi = \int_\Omega \mathbf{curl}\, u\ \phi. \end{cases}$$

To compare with the above references, we chose the finite elements of degree 2 for the velocity, of degree 1 for the pressure and of degree 2 for the stream function.

First of all, we begin to test the iterative Algorithm 4.1 with the uniform mesh method ($N = 100$) and with the stopping criteria (6.1) and (6.2) for different values of Re. We remark that it converges for Re ≤ 5000, but it does not converge for bigger values of Re. Figures 17 and 18 show the corresponding stream functions.

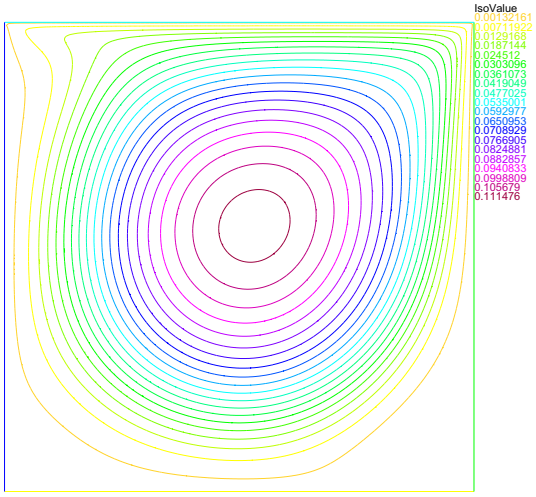

FIGURE 17. $Re = 1000$.

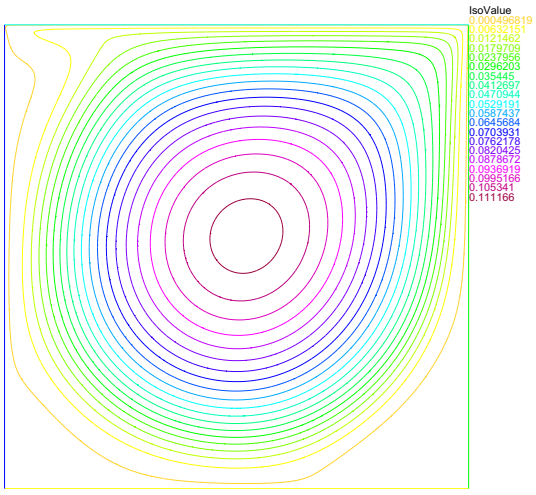

FIGURE 18. $Re = 5000$.

We slightly change (4.1) with the following: find $\mathbf{u}_h^{i+1} \in X_h$, $p_h^{i+1} \in M_h$ such that

$$\begin{aligned} &\forall \mathbf{v}_h \in X_h, \quad \nu \int_\Omega \nabla \mathbf{u}_h^{i+1} \nabla \mathbf{v}_h \, \mathrm{d}\mathbf{x} + \int_\Omega (\tilde{\mathbf{u}}_h^i . \nabla) \mathbf{u}_h^{i+1} \mathbf{v}_h \, \mathrm{d}\mathbf{x} - \int_\Omega p_h^{i+1} \operatorname{div} \mathbf{v}_h \, \mathrm{d}\mathbf{x} = \langle \mathbf{f}, \mathbf{v}_h \rangle, \\ &\forall q_h \in M_h, \quad \int_\Omega q_h \operatorname{div} \mathbf{u}_h^{i+1} \, \mathrm{d}\mathbf{x} = 0, \end{aligned} \tag{6.3}$$

where

$$\tilde{\mathbf{u}}_h^i = \frac{\mathbf{u}_h^i + \tilde{\mathbf{u}}_h^{i-1}}{2}.$$

Based on this new algorithm (6.3), the uniform mesh method with $n = 100$ converges for big values of Re.

The indicators (5.6) become

$$\tilde{\eta}_{K,i}^{(L)} = |\mathbf{u}_h^{i+1} - \tilde{\mathbf{u}}_h^i|_{1,K}, \tag{6.4}$$

$$\tilde{\eta}_{K,i}^{(D)} = h_K \left\| \nu \Delta \mathbf{u}_h^{i+1} - (\tilde{\mathbf{u}}_h^i . \nabla) \mathbf{u}_h^{i+1} - \nabla p_h^{i+1} \right\|_{L^2(K)} \tag{6.5}$$

$$+ \frac{1}{2} \sum_{e \in \mathcal{E}_{K,\Omega}} h_e^{1/2} \left\| [\nu \frac{\partial \mathbf{u}_h^{i+1}}{\partial n} - p_h^{i+1} \mathbf{n}] \right\|_{L^2(e)} + \left\| \operatorname{div} \mathbf{u}_h^{i+1} \right\|_{L^2(K)}, \tag{6.6}$$

and the upper bound in Theorem 5.4 remains the same with these new indicators.

Next, we consider the adaptive mesh algorithm with the stopping criterion (6.2) and we allow a maximum number of vertices up to 10 000. In this case, the algorithm refines in some regions of the domain and coarsens in other regions following the indicators. Figures 19–22 show the evolution of the mesh during the refinement levels for $Re = 10\,000$. We remark that, from an iteration to an other, the concentration of the refinement is on the top of the Lid where the velocity is imposed, in the two corner singularities and on the complex vorticity region (see Ref. [2]). Figures 23 and 24 show isovalues of the stream function between the uniform and adaptive mesh methods. By using the classical stopping criterion (6.1), the evolution of the meshes is similar to Figures 19–22 and the isovalues of the stream function are similar to Figures 23 and 24 for the same Re.

To show the efficiency of the proposed adaptive mesh method, we compare the uniform mesh method, the adaptive mesh method with the literature. The following Table shows the comparisons of $\|\psi\|_\infty$ with literature.

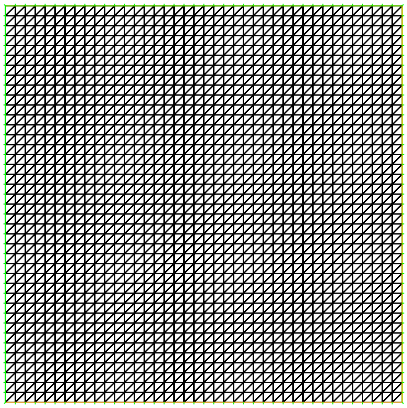

FIGURE 19. Initial mesh (Re = 10 000), number of vertices 900.

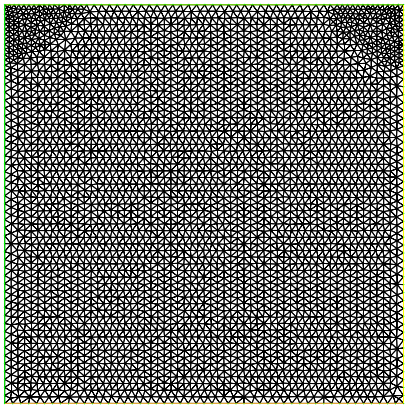

FIGURE 20. First level mesh (Re = 10 000), number of vertices 3778.

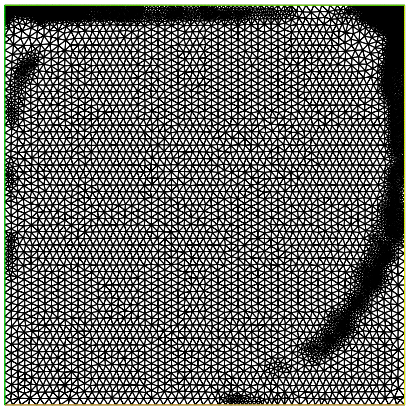

FIGURE 21. Second level mesh (Re = 10 000), number of vertices 6279.

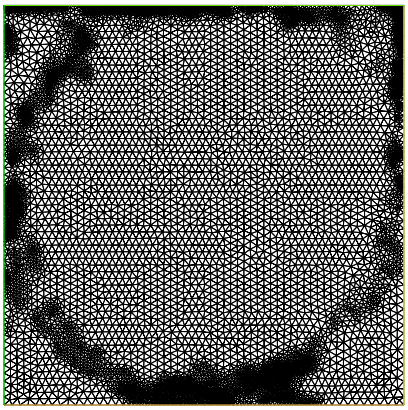

FIGURE 22. Third level mesh (Re = 10 000), number of vertices 9457.

For bigger Reynolds number, the algorithms corresponding to both methods (uniform and adaptive) do not converge for the considered meshes.

Table 4 shows that $\|\psi\|_\infty$ decreases with bigger values of Re for the uniform mesh method which is not the case for the adaptive mesh method where it remains more stable. Furthermore, the adaptive solution is comparable to the one in [16], hence it is better than the uniform solution. This is not to mention that the new stopping criterion (6.2) requires less CPU time than the classical stopping criterion (6.1) (see Tab. 3) and the adaptive method requires less CPU time than the uniform one.

In Table 5, we present the ratio of indicators on the velocity norm

$$Ind_i = \left(\frac{\left(\eta_i^{(L)}\right)^2 + \left(\eta_i^{(D)}\right)^2}{|u_h^i|_{1,\Omega}} \right)^{1/2} \simeq \frac{\eta_i^{(D)}}{|u_h^i|_{1,\Omega}}$$

with respect to the number of vertices NV with different Reynolds number.

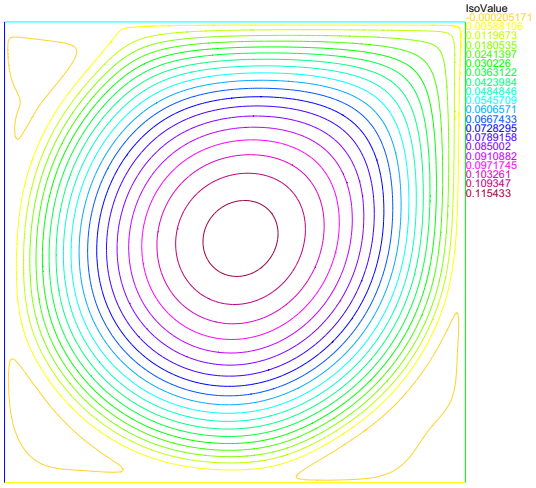

FIGURE 23. Adaptive stream function ($Re = 10\,000$).

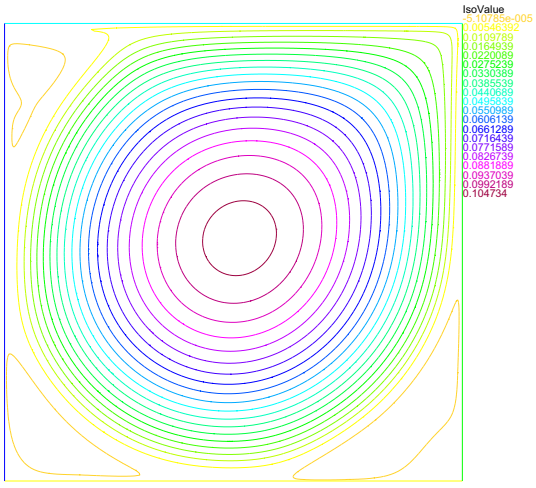

FIGURE 24. Uniform stream function ($Re = 10\,000$).

TABLE 4. $\|\psi\|_\infty$ for different Reynolds number Re and for the uniform mesh method, the adaptive mesh method with classical stopping criterion, the adaptive mesh method with new stopping criterion and the one in [16].

Method \ Reynolds Number	1000	5000	10 000	20 000	30 000
Uniform mesh method ($N = 100$)	0.114372	0.111748	0.10749	0.100236	0.0929158
Adaptive mesh method with classical stopping criterion (number of vertices up to 10 000)	0.118209	0.120131	0.118459	0.115512	0.112353
Adaptive mesh method with new stopping criterion (number of vertices up to 10 000)	0.118259	0.120127	0.118478	0.115617	0.112298
Erturk *et al.* [16]	0.118942	0.122233	0.122390	0.122084	–

TABLE 5. Ind_i with respect to the number of vertices NV for different Reynolds number.

$Re = 10\,000$			
NV	3778 vertices	6279 vertices	9475 vertices
Ind_i	0.1107	0.03201	0.02597
$Re = 20\,000$			
NV	3778 vertices	6596 vertices	9790 vertices
Ind_i	0.1358	0.03878	0.02135
$Re = 30\,000$			
NV	3778 vertices	6646 vertices	9973 vertices
Ind_i	0.1577	0.0542	0.0256

7. CONCLUSION

In this work we have derived *a posteriori* error estimates for the finite element discretization of the Navier–Stokes equations. These estimates yield a fully computable upper bound which allows to distinguish the

discretization and the linearization errors. We have shown in this work that balancing these two errors leads to important computational savings; in fact, it avoids performing an excessive number of iterations.

References

[1] R.A. Adams, Sobolev Spaces. Acadamic Press, INC (1978).

[2] R. Araya, A.H. Poza1 and F. Valentin, On a hierarchical error estimator combined with a stabilized method for the Navier–Stokes equations. *Numer. Methods Partial Differ. Eq.* **28** (2012) 782–806.

[3] I. Babuška and W.C. Rheinboldt, Error estimates for adaptive finite element computations. *SIAM J. Numer. Anal.* **4** (1978) 736–754.

[4] A. Baker, V.A. Dougalis and O.A. Karakashian, On a higher order accurate fully discrete Galerkin approximation to the Navier–Stokes equations. *Math. Comput.* **39** (1982) 339–375.

[5] E. Barragy and G.F. Carey, Stream Function-Vorticity Driven Cavity Solution using p Finite Elements. *Comput. Fluids* **26** (1997) 453–468.

[6] C. Bernardi, F. Hecht and R. Verfürth, A finite element discretization of the three-dimensional Navier–Stokes equations with mixed boundary conditions. *ESAIM: M2AN* **43** (2009) 1185–1201.

[7] F. Brezzi, J. Rappaz and P.-A. Raviart, Finite dimensional approximation of nonlinear problems, Part I: Branches of nonsingular solutions. *Numer. Math.* **36** (1980) 1–25.

[8] C.H. Bruneau and M. Saad, The 2D lid-driven cavity problem revisited. *Comput. Fluids* **35** (2006) 326–348.

[9] O.R. Burggraf, Analytical and numerical studies of the structure of steady separated flows. *J. Fluid Mech.* **24** (1996) 113–151.

[10] A.-L. Chaillou and M. Suri, Computable error estimators for the approximation of nonlinear problems by linearized models. *Comput. Methods Appl. Mech. Eng.* **196** (2006) 210–224.

[11] A.-L. Chaillou and M. Suri, A posteriori estimation of the linearization error for strongly monotone nonlinear operators. *Comput. Methods Appl. Mech. Eng.* **205** (2007) 72–87.

[12] A. El Akkad, A. El Khalfi and N. Guessous, An a posteriori estimate for mixed finite element approximations of the Navier–Stokes equations. *J. Korean Math. Soc.* **48** (2011) 529–550.

[13] L. El Alaoui, A. Ern and M. Vohralík, Guaranteed and robust a posteriori error estimates and balancing discretization and linearization errors for monotone nonlinear problems. *Comput. Methods Appl. Mech. Eng.* **200** (2011) 2782–2795.

[14] A. Ern and M. Vohralík, Adaptive inexact Newton methods with a posteriori stopping criteria for nonlinear diffusion PDEs. *SIAMJ. Sci. Comput.* **35** (2013) A1761–A1791.

[15] E. Erturk, Discussions on driven cavity flow. *Int. J. Numer. Meth. Fluids* **60** (2009) 747–774.

[16] E. Erturk, T.C. Corke and C. Gokcol, Numerical solutions of 2-D steady incompressible driven cavity flow at high Reynolds numbers. *Int. J. Numer. Methods Fluids* **48** (2005) 747–774.

[17] V. Ervin, W. Layton and J. Maubach, *A posteriori error estimators for a two-level finite element method for the Navier–Stokes equations*. I.C.M.A. Tech. Report, University of Pittsburgh (1995)

[18] V. Girault and P.-A. Raviart, Finite Element Methods for Navier–Stokes Equations. Springer-Verlag (1986).

[19] F. Hecht, New development in FreeFem++. *J. Numer. Math.* **20** (2012) 251–266.

[20] H. Jin and S. Prudhomme, A posteriori error estimation in finite element analysis. *Comput. Methods Appl. Mech. Eng.* **159** (1998) 19–48.

[21] V. John, Residual a posteriori error estimates for two-level finite element methods for the Navier–Stokes equations. *Appl. Numer. Math.* **37** (2001) 501–518.

[22] M. Kawaguti, Numerical Solution of the Navier–Stokes Equations for the Flow in a Two-Dimensional Cavity. *J. Phys. Soc. Japan* **16** (1961) 2307–2315.

[23] O. Pironneau, Méthodes des éléments finis pour les fluides. Vol. 7 of *Collection Recherches en Mathématiques Appliquées*. Masson (1988).

[24] J. Pousin and J. Rappaz, Consistency, stability, a priori and a posteriori errors for Petrov–Galerkin methods applied to nonlinear problems. *Numer. Math.* **69** (1994) 213–231.

[25] S. Prudhomme and J.T. Oden, Residual a posteriori error estimates for two-level finite element methods for the Navier–Stokes equations. *Finite Elements in Analysis and Design* **33** (1999) 247–262.

[26] R. Schreiber and H.B. Keller, Driven cavity flows by efficient numerical techniques. *J. Comput. Phys.* **49** (1983) 310–333.

[27] R. Verfürth, A Posteriori Error Estimation Techniques For Finite Element Methods. *Numer. Math. Sci. Comput.* Oxford (2013).